THE JOURNAL OF PHYSICAL CHEMISTRY B

Article

pubs.acs.org/JPCB

Binding of Hydroxyquinoline Probes to Human Serum Albumin: Combining Molecular Modeling and Förster's Resonance Energy Transfer Spectroscopy to Understand Flexible Ligand Binding

Osama K. Abou-Zied,*[,†] Najla Al-Lawatia,[†] Marcus Elstner,[‡] and Thomas B. Steinbrecher*[,‡]

[†]Department of Chemistry, Faculty of Science, Sultan Qaboos University, P.O. Box 36, Postal Code 123, Muscat, Sultanate of Oman

[‡]Department for Theoretical Chemical Biology, Institute for Physical Chemistry, Kaiserstr. 12, Karlsruhe Institute of Technology, 76131 Karlsruhe, Germany

Supporting Information

ABSTRACT: Human serum albumin (HSA) is the most abundant protein in blood plasma. It has high relevance for the lipid metabolism, and its ability to bind a large variety of natural and pharmaceutical compounds makes it a crucial determinant of drug pharmaco-kinetics and -dynamics. The drug binding properties of HSA can be characterized by spectroscopic analysis of bound probe molecules. We have recently characterized the subdomain IIA binding site of HSA using three hydroxyquinoline derivatives. In this work, we extend our study by combining data from energy transfer experiments, ligand docking, and long molecular dynamics (MD) simulations. Multiple possible binding locations are found within the subdomain IIA site, and their solvent accessibility and interactions with ligands are analyzed in detail. Binding pockets appear well hydrated during simulations, with ligands in direct contact to water molecules at all times. Binding free energies in good agreement to experiment are calculated. The HSA apoprotein is found to exhibit significant conformational flexibility over 250 ns of simulation time, but individual domains remain structurally stable. Two rotamers of Trp214 were observed on a time scale longer than 50 ns in the MD simulations, supporting the experimental observation of two fluorescence lifetime components. The flexible protein structure and heterogeneous nature of its binding sites explain the ability of HSA to act as a versatile molecular transporter. The combination of experimental and computational molecular distance information allows the conclusion that hydroxyquinoline probes bind in a binding mode similar to the anticoagulant drug warfarin.

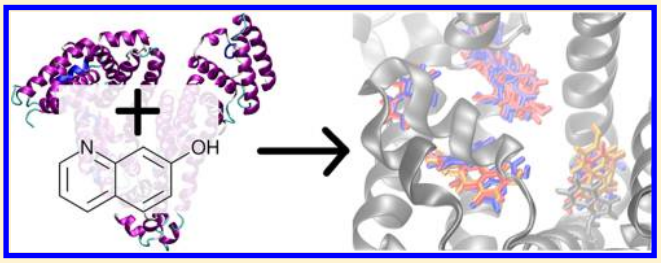

INTRODUCTION

Binding interactions that occur between proteins and low molecular weight molecules are the initiators of most of the biochemical reactions observed in vitro and in vivo.[1] One example of such interactions is the binding of small molecules including several drugs to plasma proteins. Once administered into the body, the drug is partitioned to various biological compartments and is bound to circulating carrier proteins which play a major role in affecting drug distribution in the body. One of the major carrier proteins in the body is human serum albumin, HSA, which constitutes approximately half of the protein found in human blood plasma.[2] HSA is a 585-residue monomeric protein containing three homologous helical domains, each split into A and B subdomains and arranged to form a heart-shaped molecule.[3−6] The protein is stabilized by 17 disulfide bridges[4] and contains two primary drug-binding sites.[7] Site I (or the warfarin site) is on domain 2 and prefers to bind large heterocyclic and negatively charged compounds, whereas site II (or the indole-benzodiazepine site) is located on domain 3 and is the preferred site for small aromatic carboxylic acids.[8]

The surprising capacity of HSA to reversibly bind a large variety of drugs results in its prevailing role in drug pharmacokinetics and pharmacodynamics.[9−12] Because of clinical and pharmaceutical importance, a great deal of attention has been paid to the interaction of HSA with natural or synthetic drugs.[13−17] We have recently characterized the drug binding site I of HSA in its native state using three hydroxyquinoline molecules (HQs) as local reporters.[18,19] The results indicate that intrinsic fluorescence of both tryptophan and tyrosine is useful in determining the position of the probes in the binding site. We also showed that water exists in the binding site and participates in molecular recognition and association along with Trp214 (the sole tryptophan residue in HSA).[18] The role of water in binding may stem from its behavior in the binding site which was reported to be ordered with less flexibility compared to bulk water.[20]

Received: November 13, 2012
Revised: January 5, 2013
Published: January 8, 2013

dx.doi.org/10.1021/jp311238n | J. Phys. Chem. B 2013, 117, 1062−1074

Unsurprisingly, this pharmaceutically important system has attracted considerable interest from theoretical modelers. Besides quantitative structure−activity relationship (QSAR) studies,[8,21−24] 3D-structure based atomistic modeling has been applied as well. Multiple ligand docking investigations have been presented, with ligands as varied as drug candidates,[25] fungicides,[26,27] chemotherapeutic drugs,[28] vanillin,[29] and many others,[30−34] documenting HSA's broad range of ligand interactions. Due to the large size of the 67 kDa system, fewer atomistic molecular dynamics (MD) simulation attempts have been undertaken.[35−38] A combination of ligand docking, followed by MD relaxation and energy evaluation by the approximate free energy method MM-PBSA, has been used in several of these to estimate ligand binding affinities.[39,40] To the best of our knowledge, no MD simulation of more than 10 ns length has been reported for this system, with the exception of very recent work by Paris et al. who studied HSA unfolding at elevated temperatures over 20 ns length trajectories.[36]

In this work, we will present data on the binding of three HQ compounds to HSA (Figure 1). Combining spectroscopic results from fluorescence quenching with ligand docking and extensive molecular dynamics simulations, we explore possible binding sites for the HQ probes. Distance estimates from spectroscopy can be combined with simulation results to suggest complex structures for all the three studied probes and to better understand their function. We present MD simulation data for novel HSA ligands and unprecedented length simulations on the apoprotein. We show that such long simulations are necessary to observe slower protein and ligand dynamic effects. Protein−ligand complex geometries from ligand docking calculations have been refined by conducting long molecular dynamics studies of the complexes. All-atom MD simulations are particularly useful in analyzing the involvement of water and protein flexibility in binding modes. The aim of our study is not only to advance our knowledge of HSA−small molecule interaction but also to demonstrate that the combination of experimental and theoretical work produces significant synergies in studying complex biochemical phenomena in general.

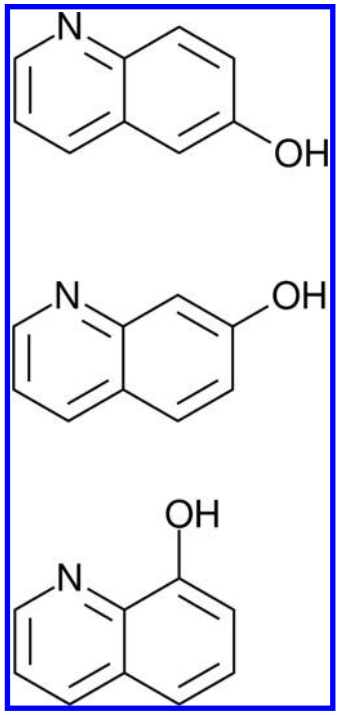

Figure 1. Three hydroxyquinoline probe molecules investigated in this work, from top to bottom, 6HQ, 7HQ, and 8HQ.

MODELS AND METHODS

Ligand Docking Calculations. Ligand docking calculations were performed using version 4.3.2 of the Autodock program.[41] Default interaction libraries and maps were used. As receptor structure, the protein chain from the 2.5 Å X-ray crystal structure of HSA cocrystallized with the drug warfarin (pdb code 1HA2) was used.[6] The grid map was constructed as a 61 point^3 lattice with a 0.375 Å point spacing, centered on the position of the warfarin molecule (which was removed for receptor preparation). Ligand docking of HQ molecules was conducted using the Lamarckian Genetic Algorithm with standard settings, conducting 100 docking runs with an initial population of 150 individuals, a maximum of 2 500 000 energy evaluations, and a maximum of 27 000 generations. The resulting docked structures were clustered with a tolerance criterion of 2.0 Å. With this setup, a complete docking calculation for one ligand was completed in about 7 h on common PC hardware.

Molecular Dynamics Simulations. System preparation for MD simulations was conducted using the leap module of the Amber modeling suite.[42,43] The protein structure was obtained from the 2.5 Å X-ray crystal structure of HSA cocrystallized with the drug warfarin (pdb code 1HA2).[6] The warfarin ligand and cocrystallized myristate molecules were removed, but resolved crystal water was maintained. Bound fatty acids were removed since, even though HSA does bind free myristic acid in vivo, experimental data are typically generated using fatty-acid-free HSA.[19] All 17 expected disulfide bridges were set, and histidine residues 464 and 535 were determined to be δ-N-protonated via visual inspection. Residues one and two, which are not resolved in the X-ray structure, were omitted from the model. For the apoprotein, the system was directly solvated in a pre-equilibrated solvent box using periodic boundary conditions so that no protein atom was closer than 15 Å from the box boundaries. For HSA−HQ complexes, the ligands were added in their binding poses obtained from ligand docking calculations before adding solvent.

MD simulations were conducted using version 12 of the Amber molecular modeling suite.[42] The protein was described using the Amber ff10 force field,[44−49] and the improved TIP4P model for Ewald calculations[50,51] was used for solvent. 6-, 7-, and 8-HQ ligands were sketched by hand, transformed into 3D-structures, and parametrized according to the gaff force field.[52] No new force field parameters needed to be introduced, and ligand partial charges were generated using the RESP methodology.[53] Systems were subjected to a standard equilibration procedure before MD simulations: an initial 100 step energy minimization with 10 kcal/mol Å^2 restraints on all non-hydrogen atoms, followed by a 100 step energy minimization with 10 kcal/mol Å^2 restraints on all nonsolvent atoms and a final 100 step unrestrained energy minimization, all conducted with 10 initial steps of steepest descent followed by 90 steps of conjugate gradient minimization. This was followed by 5 ps of NVT temperature equilibration to 298 K using a Langevin thermostat with a 10 ps^{-1} coupling constant with 5 kcal/mol Å^2 restraints on all nonsolvent atoms. The system

dx.doi.org/10.1021/jp311238n | J. Phys. Chem. B 2013, 117, 1062−1074

temperature was maintained at 298 K by a Berendsen thermostat. Density equilibration was performed in a 100 ps NPT ensemble simulation, using a weak-coupling barostat with a 10 ps coupling constant. After equilibration, all systems reached a stable temperature and density of 299 ± 1 K and 1.02 ± 0.01 g/mL.

A 2 fs integration time step was used in conjunction with the SHAKE algorithm[54,55] to maintain bonds involving hydrogen atoms at fixed lengths. Long-range electrostatics were treated using a particle mesh Ewald approach[56−58] with a 9 Å cutoff for the direct space interactions. Simulations were conducted using the GPU-accelerated version of the *pmemd* simulation engine on NVIDIA Tesla graphics cards, yielding a simulation performance of 4 ns/day on normal PC hardware, an efficiency more than an order of magnitude higher than that of a typical CPU-based simulation.[59,60] Trajectory postprocessing was conducted using the ptraj module of Amber as well as in-house custom analysis tools. Complex structures were visualized using VMD version 1.8.6,[61,62] and molecular graphics images were rendered using the POVRAY program.[63]

Experimental and Fluorescence Spectroscopy. 6HQ (98%) and 7HQ (99%) were obtained form Acros Organics. 8HQ (99%) and warfarin (98%) was purchased from Sigma-Aldrich. All HQs were recrystallized from ether, and the purity was checked by thin-layer chromatography and from their absorption and fluorescence spectra in different solvents. L-Tryptophan (99%) and L-tyrosine (98.5%) were obtained from BDH Chemicals. HSA (essentially fatty acid free) was purchased from Sigma. The buffer used was 50 mM sodium phosphate buffer, pH 7.2, and was obtained from Aldrich. Concentration of HSA in the buffer was prepared using its listed molecular weight of 66.5 kDa, and the final concentration was checked by comparing the measured absorbance with the published value (optical absorbance at 279 nm = 0.531 (1 g/L)).[64] All prepared solutions were allowed to equilibrate for 2 h before taking the measurements. Measurements were then repeated after 12 h, and no significant differences were detected.

Absorption spectra were obtained with an HP 845x Diode Array spectrophotometer. Fluorescence spectra were recorded on a Shimadzu RF-5301 PC spectrofluorophotometer. Lifetime measurements were performed using a TimeMaster fluorescence lifetime spectrometer obtained from Photon Technology International. Excitation was at 280 nm using a light-emitting diode. The system response time as measured from the scattered light was estimated to be approximately 1.5 ns. The measured transients were fitted to multiexponential functions convoluted with the instrument response function (IRF). The fit was judged by the value of the reduced chi-squared (χ^2). The experimental time resolution (after deconvolution) was approximately 100 ps, using stroboscopic detection.[65] In all the experiments, samples were contained in a 1 cm path length quartz cell, and the measurements were conducted at 23 ± 1 °C.

RESULTS

MD Simulations of the HSA apo-Protein. To study the protein dynamics and structural fluctuation in the binding site, long unrestrained MD simulations of the HSA apoprotein model were conducted. A total of 250 ns of consecutive MD simulation trajectory was produced. We observe a rapid rise in protein Cα RMSD over the first 70 ns, followed by a slower rise up to a maximum of 6.5 Å after 230 ns (Figure 2). Such a large

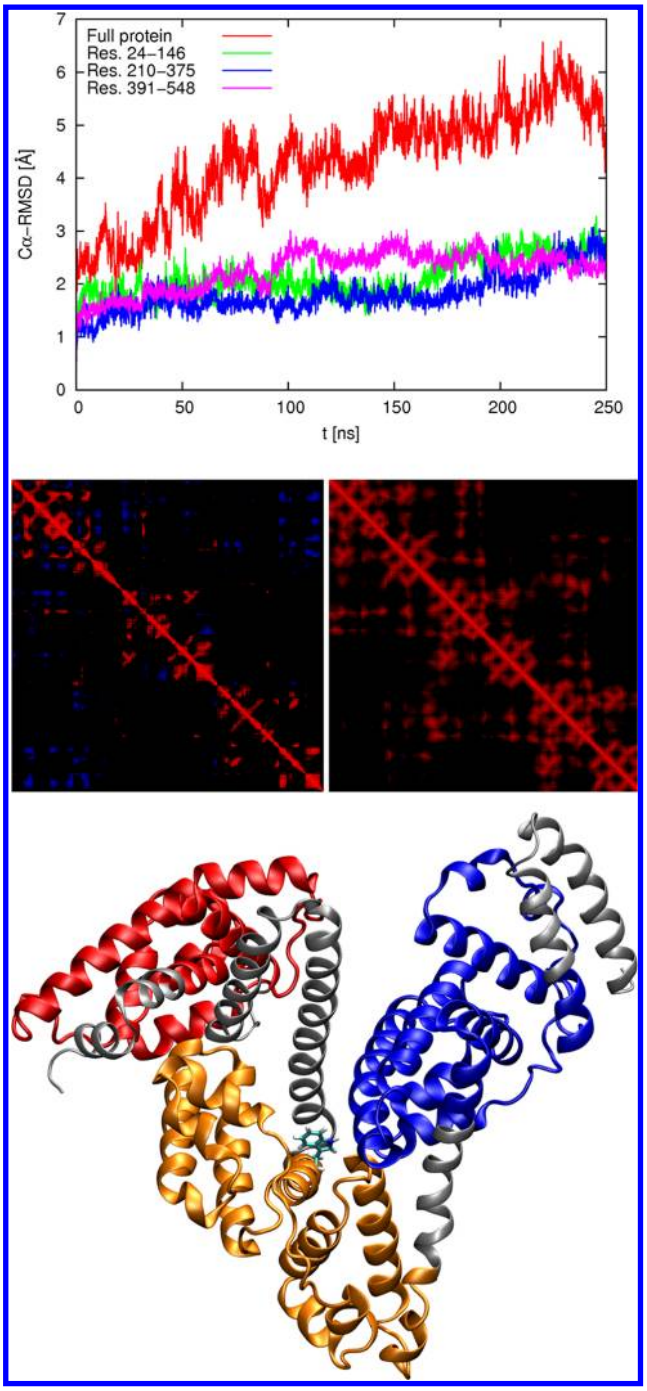

Figure 2. MD simulations of the HSA apoprotein. In the displayed orientation, the N-terminus is located in the upper left and the C-terminus in the upper right of the structure with the warfarin binding pocket at the end of the central vertical cleft. Top: For the whole protein, a large and continually rising Cα-RMSD value is found. However, RMSD values for individual protein domains remain in the 2 Å range typical for stable proteins. Middle: Cα-motion correlation (left) and distance (right) matrix for HSA. Red and blue indicate positive and negative correlation above |0.5|, while in the distance matrix the range of 0−30 Å corresponds to a change from red to black. Square features in both plots indicate compact substructures with coupled dynamics. Bottom: Our selection of three stable domains, comprising residues 24−146 (red), 210−375 (orange), and 391−548 (blue). Trp214 at the interface of domains 2 and 3 is drawn for visual guidance.

dx.doi.org/10.1021/jp311238n | J. Phys. Chem. B 2013, 117, 1062−1074

increase in RMSD would typically be considered a sign for an unstable protein structure that is insufficiently equilibrated. Computed B-factors for each protein residue also indicate large fluctuations, with an average of 137 Å^2 and median of 90 Å^2, much larger than the average B-factor from the X-ray crystal structure of 62 Å^2. However, visual inspection of the simulation trajectories shows a stable protein structure, and we observe a nearly unchanged secondary structure content of 65% helical and 13% turns over the whole simulation, compared to 74% helical and 8% turns in the starting structure. A constant radius of gyration of 28.1 ± 0.1 Å is found for the protein. Apparently, the HSA protein maintains its overall structure while permitting substantial internal dynamics.

Computing the Cα correlation of motion and distance matrices over 250 ns (Figure 2) shows patterns of residues that exhibit coupled motions. From this, we identify three domains in the protein that exhibit strongly coupled internal motions but can move fairly independently from each other. These are comprised of residues 24−146, 210−375, and 391−548, in reasonable agreement with the common partition of HSA into three domains. Recomputing RMSD values for individual domains shows much smaller structural fluctuations with curves mostly flat after 50 ns and overall RMSD values in the range of 2 Å for each domain, a value in good agreement with the expected range for a stable domain structure. To better visualize the relative and internal dynamics of these three domains, we have provided a movie of the protein structural dynamics over 250 ns in the Supporting Information (jp311238n_si_002.avi).

A clustering analysis of the simulation trajectory using the average linkage algorithm and RMS metric yielded five structural clusters (Table 1). The fact that clusters are distributed consecutively in time along the trajectory indicates that there is some remaining conformational drift in the simulation, but the high RMSD similarity that the cluster structures have suggests that this drift is small and the final structure is well equilibrated.

Table 1. Cluster Analysis of a 250 ns HSA Apo-Protein MD Simulation[a]

cluster	occurence [%]	simulation time [ns]	RMSD [Å] to C2	to C3	to C4	to C5
1	14.8	0−37	2.9	3.2	4.1	4.7
2	12.7	37−69		2.2	2.7	3.5
3	9.0	69−91			2.4	3.5
4	40.3	91−192				2.3
5	23.1	192−250				

[a]The five structural clusters appear consecutively during the simulation. RMSD values of neighboring clusters are typically below 2.5 Å.

The high structural flexibility that HSA exhibits also extends to the amino acid residues lining its potential ligand binding pockets. To illustrate this effect, we have provided a movie of the protein structural dynamics for several amino acid residues around the central Trp residue in the Supporting Information (jp311238n_si_003.avi). Notably, all four of the bulky residues around Trp214, namely, Phe211, Leu481, Val343, and Arg218, visibly explore multiple rotameric states over the course of the simulation. Additionally, Trp214 itself exists in two distinct rotamers during the simulation (Figure 3), undergoing two ca. 180° rotations, mainly changing the Cβ−Cγ dihedral angle with

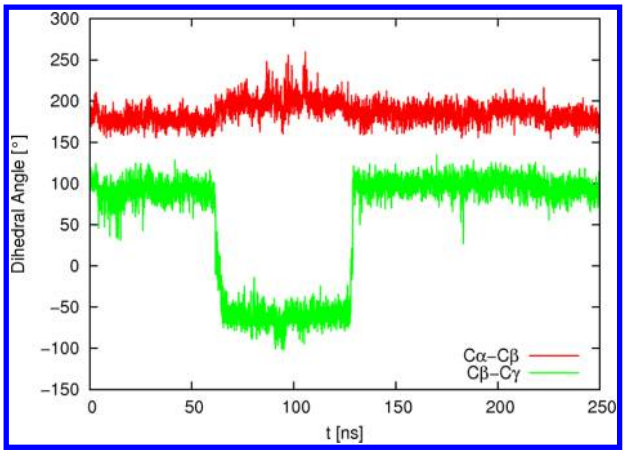

Figure 3. Dihedral time series for Trp214 during 250 ns of unrestrained MD simulations. Two major side chain reorientations are visible at ca. 60 and 125 ns, mainly changing the Cβ−Cγ dihedral angle by ca. 180° with a corresponding small adjustment of the Cα−Cβ dihedral.

smaller adjustments of the Cα−Cβ dihedral. This is in agreement with the observed two lifetime components of HSA which were assigned to two rotamers of the Trp214 residue.[19,66,67] The Trp rotation occurs on a time scale of 50 ns or more, indicating that shorter MD simulations of HSA do not capture such essential dynamics phenomena. Not only the amino acid side chains but also their backbone scaffold undergo large structural fluctuations, while maintaining its secondary structural elements and overall fold. These results, along with the biexponential nature of the HSA fluorescence decay, constitute strong support for the ground state heterogeneity that is associated with a degree of flexibility of the Trp214 side chain to adapt two different rotamers (more discussion is included in the Supporting Information). The binding side is well hydrated, with ca. 20 solvent molecules within 5 Å of Trp214 at any time during the simulation. Overall, the MD simulation of the apoprotein shows evidence for a large and flexible multidomain enzyme containing large and well-hydrated binding pockets. This is in good agreement with the ability of HSA to reversibly bind a variety of small drug molecules. Hydration of the binding domain is consistent with the observed HSA fluorescence which peaks at around 340 nm, typical of a partially buried Trp residue.[19,66−68]

Choice of X-ray Crystal Structure. For the following ligand docking calculations, the choice of X-ray crystal structure for the receptor is important. We have chosen the X-ray crystal structure of HSA cocrystallized with the drug warfarin[6] (pdb code 1HA2) among the many available deposited structures. To avoid biasing our results by choice of receptor structure, we conducted MD simulations of docked complexes, described below. To demonstrate the ability of MD simulations to sufficiently explore the conformational space of HSA to reduce starting structure bias, we compare MD simulations of three additional HSA crystal structures with various ligands or no ligand. The structures corresponding to pdb entries 1GNJ,[69] 2BXF,[9] and 3JRY[70] with cocrystallized arachidonic acid, the drug molecule diazepam, and no ligand, respectively, were chosen, for a selection of high-quality structures with a wide variety of bound ligands.

From these, solvated apo-HSA models were prepared and equilibrated as described for the 1HA2 structure above. Then, 10 ns length unrestrained MD simulations were conducted for

dx.doi.org/10.1021/jp311238n | J. Phys. Chem. B 2013, 117, 1062−1074

all three models and compared to the structure of the apoprotein based on the 1HA2 structure, also after 10 ns of simulation time. For all four systems, total protein RMSD values rose by 2.5−4.2 Å over 10 ns, similar to the situation in Figure 2. Of higher interest are the backbone RMSD values of domain 2 which contains the warfarin binding pocket. These are summarized in Table 2. We see that for all four cases the domains remain close to their starting structures with RMSD values below 2 Å, with the exception of the 1GNJ structure where RMSD values rise to ca. 2.5 Å, possibly due to the removal of multiple large lipid molecules during model preparation.

Table 2. RMSD Values of Various HSA X-ray Crystal Structures after Equilibration and 10 ns MD Simulation[a]

simulated structure from pdb entry	$RMSD_{1HA2}$ [Å]	$RMSD_{1GNJ}$ [Å]	$RMSD_{2BXF}$ [Å]	$RMSD_{3JRY}$ [Å]
1HA2	1.37	1.33	1.37	1.42
1GNJ	2.35	2.31	2.42	2.47
2BXF	1.63	1.61	1.50	1.58
3JRY	1.19	1.18	1.11	1.15

[a]RMSD values were measured for domain 2 as defined in Figure 2, namely, the backbone atoms of residues 210−375. Results show that in each simulation the overall domain structure is fairly well maintained. Furthermore, already after 10 ns simulation time, the difference between any structure and its starting crystal structure is comparable to its difference to any other crystal structure. This indicates that long MD simulations are well suited to remove starting structure bias for HSA and that all four simulations explore similar regions of conformational space.

Notably, after only 10 ns of equilibration time, all four structures exhibited very similar RMSD values compared to any of the four starting X-ray crystal structures (as well as to each other). This indicates that any starting structure bias is efficiently removed after MD simulations. Apparently, strongly overlapping conformational ensembles are explored by all simulations, independent from their starting coordinates. This finding will be exploited below when MD simulations of docked complexes are conducted for further equilibration.

Ligand Docking Results. To predict possible binding modes for HQ ligands to the HSA receptor protein, ligand docking calculations were conducted for 6-, 7-, and 8-HQ, using Autodock as described above. The main results are summarized in Table 3. Multiple possible binding positions are found for all three compounds, eleven for 6HQ, four for 7HQ, and twelve for 8HQ. The number of individual docking results clustered together into one binding pose is widely different for all compounds and ranges from 1 to 75 (average of 11 ± 18). The three HQ compounds are structurally similar isomers, each with one potential hydrogen bond donor and acceptor group. It is therefore unsurprising that very similar docking scores are found for all compounds, of on average −5.42 ± 0.32 kcal/mol. It is not possible to identify any one of the three compounds to have a higher or lower predicted binding strength than the other two.

The distribution of the resulting docked ligand positions in the receptor interior shows an interesting pattern: Four distinct binding pockets are found, arbitrarily labeled here as pockets 1 to 4. The distribution of the 27 total ligand placements over these four pockets is shown in Figure 4 (Top, left), where pocket 1 corresponds to the right placements, pocket 2 to the top, pocket 3 to the bottom, and pocket 4 to the left bundle of ligand positions. 6HQ and 8HQ were placed in all four pockets, and 7HQ was placed only in pockets 1 and 3. Pockets 2 and 3 comprise the majority of docked placements (14 and 7, respectively). See Table 4 for a list of amino acid residues directly lining the binding pockets.

Table 3. Ligand Docking Results for Three HQ Ligands and Warfarin Binding to HSA[a]

compound	docking	cluster size	$\Delta G_{(AD)}$	pocket
6HQ	1	4	−6.02	2
	2	8	−5.72	2
	3	7	−5.68	1
	4	11	−5.6	2
	5	2	−5.59	4
	6	1	−5.48	2
	7	6	−5.24	2
	8	58	−5.18	3
	9	1	−5.07	2
	10	1	−4.99	2
	11	1	−4.97	3
7HQ	1	75	−5.53	1
	2	9	−5.31	1
	3	15	−5.19	3
	4	1	−5.04	3
8HQ	1	13	−6.12	4
	2	2	−5.8	2
	3	4	−5.74	2
	4	1	−5.68	2
	5	1	−5.6	2
	6	1	−5.5	2
	7	25	−5.45	3
	8	39	−5.32	1
	9	7	−5.32	3
	10	1	−5.15	2
	11	5	−5.1	3
	12	1	−5.01	2
warfarin	1	2	−6.99	3 (3.1)
	2	55	−6.91	3 (1.0)
	3	1	−7.01	3 (2.7)
	4	4	−6.71	3 (2.6)
	5	1	−6.46	1 (6.5)
	6	26	−6.21	3 (2.7)
	7	1	−6.35	3 (2.8)
	8	4	−6.05	3 (1.9)
	9	6	−5.98	1 (5.4)

[a]For 6HQ, eleven docking poses were found, for 7HQ four, for 8HQ twelve, and for warfarin nine. "Cluster Size" indicates how many individual ligand positions comprise a result cluster; binding free energies are given in kcal/mol; and "Pocket" indicates which of the four distinct binding pockets this binding pose occupies. For warfarin, the bracketed number in the last column gives the RMSD value in Å of the docked pose compared to the known warfarin binding mode from X-ray crystallography.

Pocket 1 is situated in domain 2, at the bottom of the cavity separating domains 1 and 3. Ligands are placed in van der Waals contact with the amino acid residue Trp214 in a π-stacked complex. Pocket 1 is lined by both polar (Lys199, Ser202) and nonpolar residues (Leu 198, Phe211, Val455). Pocket 2 lies at the interface between domains 1 and 2 and accommodates the largest number of ligand placements, namely, 14. The binding pocket lies close to the protein surface and is lined mostly by polar (Lys106, Gln29) and slightly polar (Tyr148, Tyr150, Cys246) residues. Binding

dx.doi.org/10.1021/jp311238n | J. Phys. Chem. B 2013, 117, 1062−1074

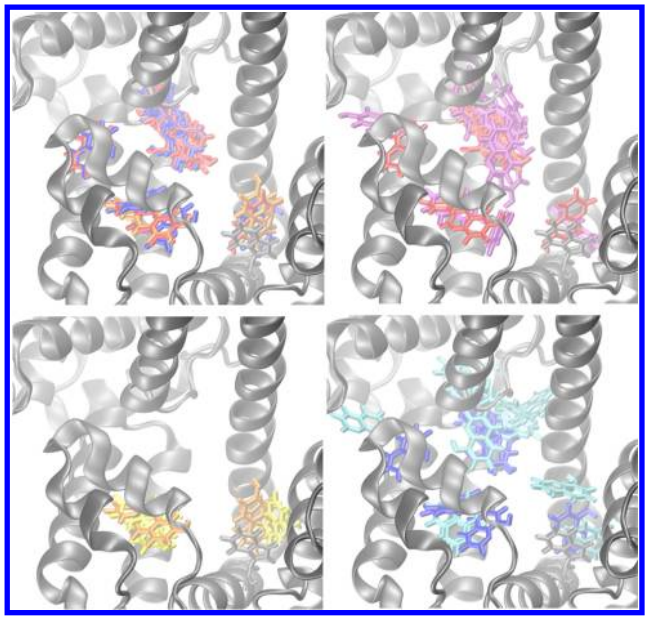

Figure 4. Ligand binding modes predicted from docking calculations and MD complex relaxation. The protein structure is drawn in gray cartoon representation, and in the lower right residue Trp214 is also shown for visual guidance. Multiple ligand placements from docking and final structures from MD simulations are plotted simultaneously. Top, left: binding modes for 6HQ (red), 7HQ (orange), and 8HQ (blue) from Autodock ligand docking calculations. Four distinct binding pockets are found, of which the lower central one is equivalent to the warfarin binding site from the X-ray crystal structure. Top, right: Binding modes of eleven ligand placements of 6HQ from docking (red) and after equilibration and 25 ns of unrestrained MD simulation (purple). Bottom, left: Binding modes of four ligand placements of 7HQ from docking (orange) and after equilibration and 25 ns of unrestrained MD simulation (yellow). Bottom, right: Binding modes of twelve ligand placements of 8HQ from docking (blue) and after equilibration and 25 ns of unrestrained MD simulation (cyan). One of the 8HQ ligands moves from binding site three to one during MD equilibration. All other ligand placements remain in their binding pockets but typically undergo significant conformational rearrangement.

pocket 3 is equivalent to the warfarin binding site from the X-ray crystal structure. As described in ref 6, this pocket is situated in the center of domain 2 and offers interactions with both nonpolar residues (Leu260, Ile264, Ile90) as well as polar ones (Arg257, His242). Pockets 1 and 3 are open and connected to each other via the central protein cleft. Binding pocket 4 is also situated in domain 2, on the protein surface facing domain 1. This is the most shallow binding pocket predicted, and only two ligand placements were found in it. All four binding pockets lie close to the protein surface and suggest easy solvent accessibility of bound ligands. Overall, ligand docking results suggest that HSA is capable of binding different HQ ligands, possibly in multiple binding orientations, with an overall moderate binding strength.

Since ligand docking calculations only provide a static picture of binding and approximate solvation models, in the following we have applied long unrestrained MD simulations to better understand the dynamics of the complexes.

Warfarin Redocking. As a positive control for the ability of our ligand docking approach to predict likely binding sites for ligands to HSA, we conducted a redocking experiment, using the same simulation parameters as in HQ docking above, with the cocrystallized warfarin (WAR) molecule removed from the 1HA2 X-ray structure during receptor preparation. The results are summarized in Table 3. Overall, nine distinct ligand placements are predicted in the docking calculations, with widely differing numbers of docked poses in any cluster. As for the HQ molecules, moderate binding strengths of on average −6.62 kcal/mol were found that do not allow the determination of one clearly favored binding pose.

Two large clusters account for the majority of placements, both of which are structurally close to the known binding mode of WAR from X-ray crystallography. Cluster 2, which accounts for 55% of all docking placements, perfectly superimposes on the X-ray reference structure with an RMSD value of less than 1 Å (Figure 5). The majority of placements lie in pocket 3 with two clusters in pocket 1. The finding of multiple clusters of docking poses in pocket 3 is caused by the higher conformational flexibility of the WAR molecule which prevents clustering for some placements despite very small center of mass distances. No docking results placing WAR in pockets 2 and 4 were found.

The positive control redocking calculation shows that our ligand binding mode prediction approach using Autodock is capable of finding the correct binding mode for the known ligand WAR. Most docking results are within the WAR binding pocket, and even the precise details of ligand rotation and internal conformations are predicted correctly in a majority of placements. As is typical for ligand docking calculations, additional binding poses are found that could correspond to false positive predictions or alternate binding modes. Similar to the case of the HQ molecules above, WAR is placed in more than one binding pocket of HSA, with placements in pocket 3 (the known WAR binding site) predominant and additional placements in pocket 1.

WAR and HQs are somewhat similar molecules composed mainly of rigid fused aromatic cores and a few polar groups capable of hydrogen bonding. The success of the WAR

Table 4. Binding Pockets and Ligand Docking Placement Distribution[a]

		ligand placements
binding pocket	residues	total/6HQ/7HQ/8HQ
1	198, 199, 202, 211, 214	4/1/2/1
2	29, 106, 148, 150, 151, 245, 246, 248, 250	14/7/0/7
3	241, 242, 257, 260, 261, 264, 290	7/2/2/3
4	150, 152, 254, 258, 261, 283, 286, 287	2/1/0/1

[a]Pocket numbers have been arbitrarily chosen. "Residues" gives the amino acid residues in van der Waals distance (2.5 Å) of a representative ligand placement in the respective binding pocket. 6HQ and 8HQ were placed in all four pockets, and 7HQ was placed only in pockets 1 and 3. Pocket 1 places ligands into van der Waals contact with amino acid residue Trp214, and pocket 3 corresponds to the warfarin binding site from the X-ray crystal structure.

dx.doi.org/10.1021/jp311238n | J. Phys. Chem. B 2013, 117, 1062−1074

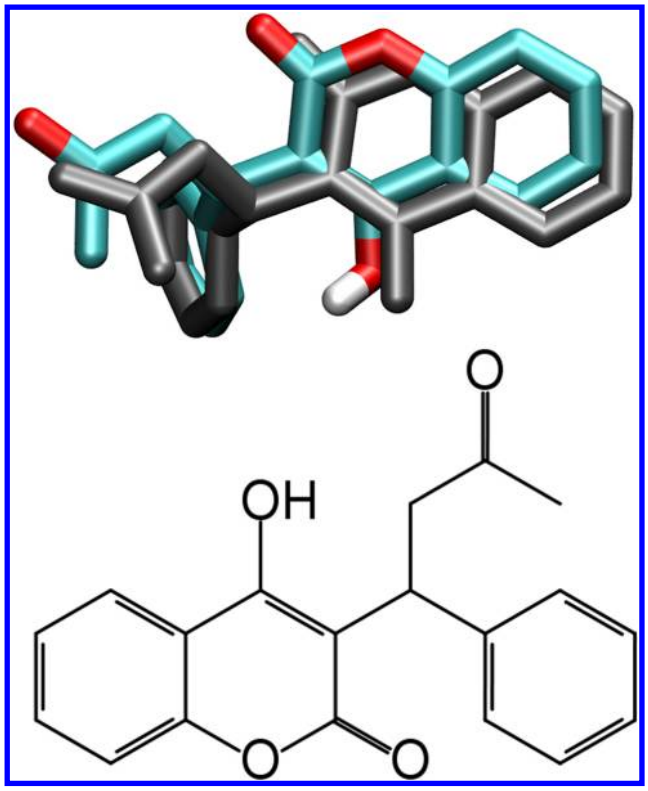

Figure 5. Comparison of warfarin binding modes from X-ray crystallography and predicted from Autodock docking calculations. Top: The largest cluster of docked placements (in color) lies in pocket 3 and superimposes very well on the warfarin binding position known from experiment (gray), with an RMSD value of 0.98 Å. The placement shown corresponds to cluster 2 containing 55% of docking predictions. Eight additional binding modes were found for warfarin, most of them also in pocket 3 (see text for details). Bottom: Structure of warfarin.

redocking calculation suggests that docking the smaller and less flexible HQ probes into HSA will also lead to reliable predicted binding modes.

Molecular Dynamics Complex Refinement. Docked complex structures of all 27 predicted HQ ligand binding modes were extracted and transformed into MD complex models. These were subjected to a standard equilibration protocol after which a 25 ns length unrestrained MD simulation was conducted for each complex. The protein secondary structure elements did not change significantly in the complex simulations, compared to the apoprotein results above. During the course of all simulations, we observe significant and variable dynamics of the ligands in their respective binding pockets. All HQ molecules remain bound to HSA. No ligand leaves its original binding pocket, with the exception of one docked placement of 8HQ, which moves from pocket 3 to pocket 1 right after equilibration (these two binding pockets are connected via a solvent accessible cleft). The amount of bound ligand dynamics was measured as the RMSD value with respect to the initial docked structure. Note that it is not possible to unambiguously separate this RMSD value into contributions of ligand motion within the binding site and of internal protein dynamics that change the shape and position of the binding pocket with respect to the rest of the protein. To obtain an RMSD value that mostly describes ligand motion, we measure ligand RMSD after a best rotational and translational fit of only the amino acid residue Cα atoms that form the binding pockets (see Table 4), instead of a fit for the whole protein which is more common in ligand binding analysis.

To better analyze the results, proper statistics are needed. Since ligand docking calculations yielded typically 2 or less placements of a ligand in a binding pocket (with the exception of pocket 2 for 6HQ and 8HQ, see Table 4), there is insufficient data to discuss the binding of each ligand into each binding pocket in detail. Since the three HQ ligands are very similar structurally and fairly evenly distributed over the four pockets, we will from here on discuss binding properties as averages for all simulations of any ligand in that pocket. The results should therefore not be overinterpreted since ligands are not perfectly equally distributed among binding pockets. For example, most ligand placements in pocket 1 are from 7HQ, so any differences found between pocket 1 and the other three could stem either from properties of the binding pocket or from properties of the 7HQ ligand.

The complex trajectory analysis shows significant ligand motions. Overall, final complex structure RMSD values after 25 ns of MD were 4.9 ± 3.1 Å. Only 7 out of 27 simulations had ligand binding modes similar (defined as within 3 Å) to the initial structure. Average ligand mobility in terms of RMSD was comparable for binding pockets 1, 2, and 3, at 4.8, 4.1, and 4.1 Å, but higher for pocket 4, at 7.1 Å. This, together with the fact that only two ligand placements were found for pocket 4, suggests that this is the least stable binding site for HQ ligands found. Both high ligand RMSD values, combined with ligands mostly remaining in their initial binding pocket, can be explained by comparably free rotation of the flat HQ molecules in the pockets and by the fact that binding pockets are typically larger than the HQ ligands, allowing for easy conformational rearrangement. Figure 4 shows the increasing flexibility of ligand positions when comparing initial docked positions to the end states of MD simulations. Clearly, the full conformational flexibility of both ligand and protein allows for a substantial exploration of conformational space around the starting structures. We provide a visualization of the trajectory of the ligands in their binding pockets in the Supporting Information (jp311238n_si_004.avi).

Polar interactions between ligands and protein are crucial determinants of their binding properties. We have monitored H-bonds between HQ ligands and HSA over the course of all complex simulations. We find multiple H-bond interactions for all bound ligands, but with substantial variation in intensity. These range from forming 0.04 H-bonds on average to 2.07 H-bonds (since HQ can form multiple H-bonds simultaneously, the average can be above 1). Over all MD snapshots, the three ligands and four binding sites form 0.8 ± 0.5 hydrogen bonds. In pockets 2 and 3, more H-bonds are found (on average 1.06 and 0.94, respectively) than for pockets 1 and 4 (0.50 and 0.60, respectively), indicating stronger polar interactions for binding pockets 2 and 3. Likewise, 6HQ forms on average 1.14 H-bonds, more than 8HQ and 7HQ (0.78 and 0.57, respectively). Still, these results suggest that pockets 2 and 3 allow ligands to form multiple hydrogen bonds to the protein, while pocket 1 appears slightly more hydrophobic.

Solvent access to a bound ligand is likewise important for its binding properties. When monitoring the number of hydrogen bonds formed between ligands and solvent, substantial hydration of ligands in all binding sites is found. On average, 0.84 ± 0.65 hydrogen bonds to solvent are present at any time. The ligand hydroxyl groups account for 78% of H-bonding interactions, compared to 22% for the nitrogen group.

Solvation differs between binding pockets, with 0.52 hydrogen bonds on average in pocket 1, substantially less than in pockets 2, 3, and 4 (0.86, 1.04, and 0.92, respectively). Still, even though pocket 1 appears slightly less solvent exposed than the other three, in all cases ligands are solvent-accessible in HSA, pointing to the important role water molecules may play in stabilizing bound ligands. Figure 6 shows the distribution of water molecules around two exemplary MD snapshots, one for 6HQ in a binding mode that forms multiple solvent H-bonds (on average 2.12) and the other for 7HQ in pocket 1, which forms fewer (on average 0.21) but is still in close contact with water molecules most of the time. Clearly, ligands bound to HSA are significantly exposed to solvent, and binding pockets are accessible enough to be at least partially water filled.

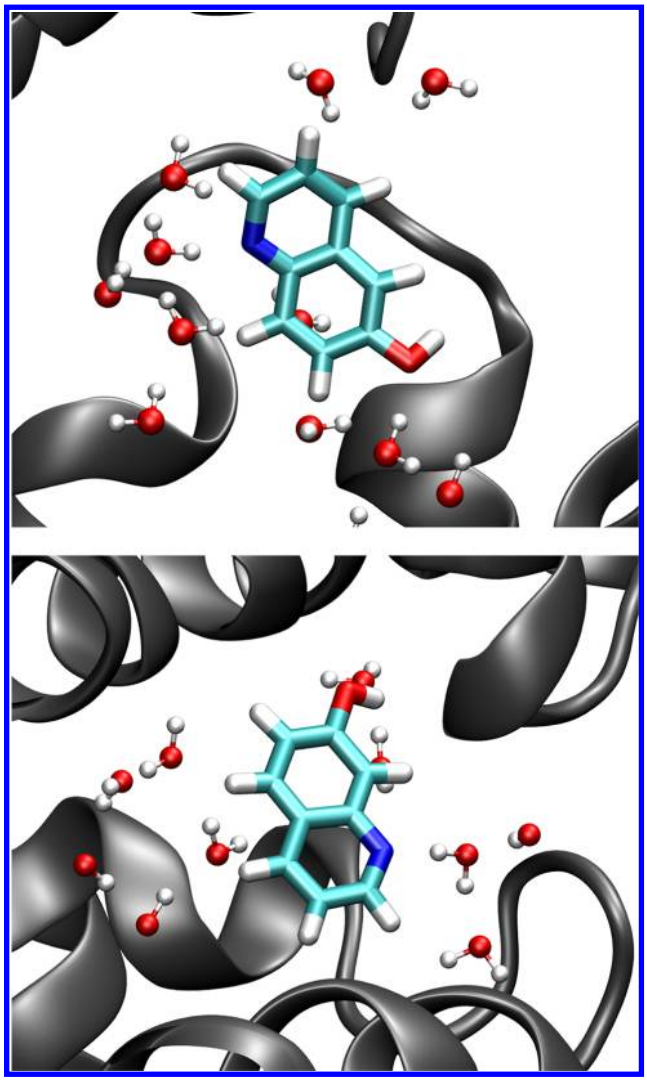

Figure 6. Water molecule distribution around bound HQ ligands. Two exemplary snapshots for 6HQ in pocket 3 (top) and 7HQ in pocket 1 (bottom) are shown, corresponding to the end state of the MD simulations in which the most and least solvent H-bonds were found, respectively. Water molecules up to 5 Å away from the ligand are shown. Some protein parts (in gray cartoon representation) are omitted for visual clarity.

Computing accurate ligand binding free energies for the different ligands to the receptor pockets would be very valuable in determining their in vitro binding modes, especially since ligand docking binding scores turned out to be non-discriminatory (arguably correctly so, see Discussion). However, the calculation of reliable binding free energies is a challenging task even in small, highly stable, and well-characterized systems.[71−78] MM-PBSA is a popular, approximate, and fast free energy method that has been successfully applied to HSA before,[40] but it was shown to be only moderately reliable in many other cases.[79,80] We have conducted MM-PBSA free energy calculations for all HQ ligands over the last 10 ns of their simulations, equivalent to 200 conformational snapshots, using standard parameters in Amber for MM-PBSA and MM-GBSA. As is common in this type of evaluation, no entropy contribution was included; instead, the binding entropy was estimated as equal for all ligands in all binding modes. Binding free energy results of −12.2 ± 5 kcal/mol and −17.2 ± 4 kcal/mol were found on average, for a Poisson−Boltzmann and Generalized Born treatment of implicit solvation.

Very similar binding energies were found for all pockets in both cases, with the exception of slightly lower (by 1−2 kcal/mol) binding scores for pocket 4. In all cases, a strong van der Waals contribution to binding of −23.4 ± 3 kcal/mol was found, as expected for the partially hydrophobic HQ molecules. Note that, due to the missing entropy contribution in MM-PBSA scores, binding energies can not be directly compared to experimental values. Still, the magnitude of the binding free energy scores $\Delta G^0_{\mathrm{MM-PBSA}}$ of −20 kcal/mol or weaker points to at best moderately strong binding by HQ ligands. The large difference in free energies computed with the PB and GB solvent models points to the at best qualitative nature of the results. Nevertheless, the MM-PBSA results overall can be interpreted as agreeing well with the ligand docking binding scores: all ligands are predicted to bind comparably strong, and no binding pocket can be identified as favored. Surprisingly, incorporating complex flexibility from long MD simulations into the binding energy estimation did not yield a marked improvement of results.

For the interpretation of fluorescence quenching spectra, information about the distances of bound ligands to fluorescent protein residues of HSA, namely, Trp214 and its 18 Tyr residues, is of high importance. These distances, specifically the ligand to amino acid residue center of mass distance, have been measured for all simulations. Since all ligands are of comparable size and share the same binding pockets, we provide average values for the four binding pockets only (Table 5). The four pockets differ markedly in their distance to Trp214, ranging from ca. 6 to 27 Å in the order 1 < 3 < 2 < 4. On the other hand, distances to the nearest Tyr residue were lower and tended to be uniformly ca. 11 Å, with the exception of binding pocket 2, where smaller distances were found, since Tyr146 and

Table 5. Average Distances of Ligands in the Four Binding Pockets to Fluorescent Amino Acid Residues[a]

binding pocket	*d*(Trp214) [Å]	*d*(Tyr) [Å]
1	5.9	12.7 (450, 339)
2	17.1	5.5 (146, 148, 28)
3	10.2	10.6 (148, 261)
4	26.6	10.1 (148)

[a]Shown are the distances to the sole Trp214 residue of HSA and to the closest Tyr residue. Numbers in brackets indicate all tyrosine residues that were closest to a ligand in at least one simulation.

dx.doi.org/10.1021/jp311238n | J. Phys. Chem. B 2013, 117, 1062−1074

Tyr 148 form part of this binding pocket. This distance distribution can be used together with fluorescence quenching data to decide which binding pockets are most likely to be occupied by HQ ligands (see Discussion).

We tested convergence of our results by extending the length of the MD simulations to 50 ns for five randomly selected complexes. In all cases, very similar results compared to the shorter simulations were observed. Ligand RMSD values and interactions with the binding site did not change significantly, and ligands still remained in their initial binding pockets in all cases.

Fluorescence Spectra and Lifetimes. The intrinsic fluorescence of HSA is a useful tool to detect the presence of the ligand near Trp214.[19,67,81] Figure 7 shows the fluorescence

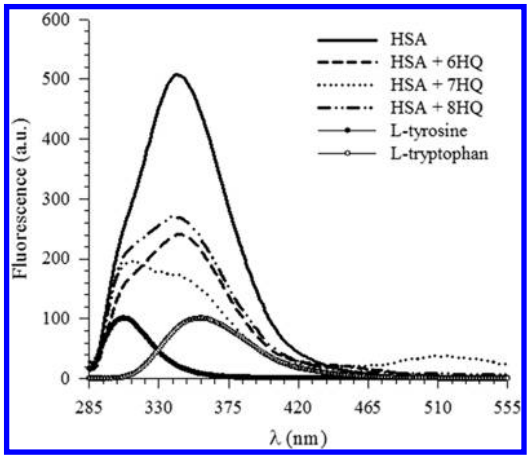

Figure 7. Fluorescence of HSA in the absence and presence of HQ ligands. Fluorescence of L-tyrosine and L-tryptophan is also shown. The concentration of all species was 0.1 mM in 50 mM phosphate buffer of pH 7.2. λ_{ex} = 280 nm. The fluorescence peaks of L-tyrosine and L-tryptophan are normalized to reflect their positions.

spectra of HSA measured in the absence and presence of HQ ligands. Quenching of HSA fluorescence in the presence of HQs indicates that the three probes bind close to Trp214. The degree of quenching of the Trp214 fluorescence is also different for each HQ probe, implying different interactions between Trp214 and the probes. This quenching depends on the degree of overlap between the fluorescence of the donor (Trp124) and the absorption of the acceptor (HQ) and on the molar absorption coefficient (ε) of the latter (see refs 19, 67, and the Supporting Information for details). The fluorescence spectrum of L-tryptophan in buffer is red-shifted with respect to that of HSA, indicating a less polar environment around the Trp214 residue in native HSA compared to buffer.[19,67] The peak at 510 nm in Figure 7 is due to fluorescence from the zwitterion tautomer of 7HQ. The stability of this tautomer indicates the presence of water close to the probe and confirms the hydrated nature of the binding site.

The observed fluorescence quenching indicates the existence of an energy transfer mechanism between Trp214 and HQs. Using Förster's theory for resonance energy transfer (FRET),[82,83] we estimated the energy transfer efficiencies and the apparent distance (R_{DA}) between Trp214 and each of the HQ molecules (detailed calculations are included in the Supporting Information). The data are summarized in Table 6. The donor-to-acceptor distance in all complexes indicates a major contribution from static quenching according to Förster's

Table 6. Calculated Fluorescence Parameters for the HSA–HQ Complexes[a]

	Trp214–6HQ	Trp214–7HQ	Trp214–8HQ
efficiency of energy transfer (% E)	53	66	47
donor–acceptor distance (R_{DA} [Å])	21	20	18
quenching rate constant (k_q [10^{-12} M^{-1} s^{-1}])	1.4	3.0	1.4
equilibrium binding constant (K [10^{-5} M^{-1}])	1.1 ± 0.1	1.6 ± 0.2	1.0 ± 0.1
number of binding sites (m)	1.1 ± 0.1	1.2 ± 0.1	1.2 ± 0.1

[a]The FRET parameters were calculated using the fluorescence spectra shown in Figure 7.

theory.[66,83] This is supported by the calculated quenching rate constants using the Stern–Volmer relation in which the values of k_q (Table 6 and Supporting Information) are greater than the maximum dynamic collisional quenching rate constant of various kinds of quenchers with biopolymers.[84] We further clarified this point by measuring the fluorescence lifetimes of HSA. Quenching of the Trp214 fluorescence by HQs resulted in shortening of the measured fluorescence lifetimes of HSA (Table 7). The two measured lifetime components are due to

Table 7. Fluorescence Lifetimes for the HSA–HQ Complexes using λ_{ex} = 280 nm[a]

	τ_1 [ns]	τ_2 [ns]	χ^2
HSA	6.71 ± 0.10 (0.96)	1.39 ± 0.28 (0.04)	1.01
HSA + 6HQ	5.54 ± 0.17 (0.94)	0.63 ± 0.27 (0.06)	1.10
HSA + 7HQ	4.69 ± 0.16 (0.92)	0.63 ± 0.24 (0.08)	0.73
HSA + 8HQ	6.03 ± 0.22 (0.91)	0.71 ± 0.18 (0.09)	0.77

[a]Relative contributions are listed in parentheses.

two different rotamers of Trp214 as mentioned above. If we compare the effect of the quenchers (HQs) on the fluorescence intensity of Trp214 and its average fluorescence lifetime, it is apparent that the fluorescence intensity dropped about 50% upon the addition of HQs (65% in the case of 7HQ), whereas the average fluorescence lifetime of Trp214 is slightly shortened in the presence of HQs. This is a manifestation of the dominant role of static quenching (lifetime is not affected) compared to collisional quenching (where lifetime would be affected).[66] The slight decrease in the average fluorescence lifetime of Trp214 in the presence of HQs is then due to a small contribution from collisional quenching. This may explain the docking results in which multiple possible binding positions are found for all three HQs. The exchange between these close positions can then be viewed in this regard as a slight motion of the probe from one position to another within the same cavity or two closely connected cavities like pockets 1 and 3, induced by the flexibility of the protein, while the distance from Trp214 is only changing slightly.

From the change in the fluorescence of Trp214 upon a gradual addition of HQs, we calculated the equilibrium binding constants (K) for the HSA–HQ complexes along with the number of binding sites (m).[19,67,85] The results are included in Table 6. The values of m indicate that in each case the probe is located in one binding site. The results, along with the quenching results, indicate that HQs bind only in subdomain IIA in HSA. Increasing the concentration of the probes to three

dx.doi.org/10.1021/jp311238n | J. Phys. Chem. B 2013, 117, 1062–1074

times that of the host HSA produces the same m value which points to the high affinity of the probes for binding in subdomain IIA.

Finally, upon quenching of the Trp214 fluorescence, a second peak at 308 nm is clearly distinguished in Figure 7. This peak is due to tyrosine fluorescence[67] (this is evident from comparing its fluorescence peak position with that of L-tyrosine in buffer). The slight decrease in the fluorescence intensity at 308 nm indicates that the probes are also close to tyrosine residues. Estimating the Tyr−HQ distances is complicated in this case since there are 18 tyrosine residues in HSA and, as mentioned above, there is more than one tyrosine close to each probe in any predicted binding position.

Competitive Binding of HQs and Warfarin. To better determine the location of HQs in the binding site, we performed site-competitive displacement experiments with a specific site marker for the subdomain IIA cavity. We examine here the effect of the presence of WAR on the HSA:HQ binding. Figure 8 displays the fluorescence spectra of the

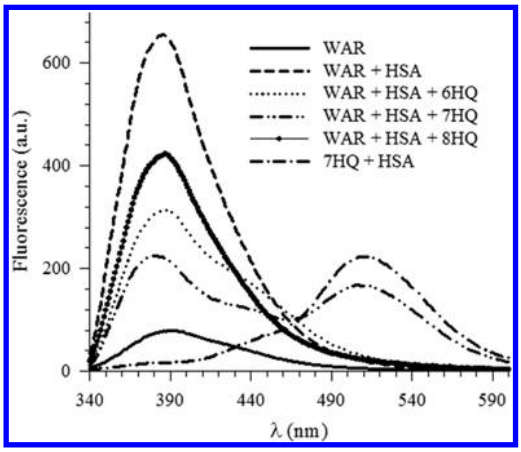

Figure 8. Fluorescence spectra of warfarin, warfarin:HSA binary mixture, warfarin:HSA:HQs ternary mixtures, and 7HQ:HSA binary mixture. The concentration of all species was 0.1 mM in 50 mM phosphate buffer of pH 7.2. λ_{ex} = 330 nm.

equimolar binary mixture WAR:HSA and that of the ternary mixtures WAR:HSA:HQs after excitation at 330 nm. The intensity of WAR fluorescence in the ternary mixtures is less than that in its binary complex with HSA. The largest effect on the WAR fluorescence was observed in the ternary mixture with 7HQ where the fluorescence intensity of WAR dropped by a factor of approximately 3. The results can be interpreted as a displacement of WAR by HQ because the two molecules share a common binding site, with a higher affinity toward 7HQ. The decrease in the WAR fluorescence in the presence of HQ in the ternary mixture can be explained by the exiting of WAR to buffer.[86] Fluorescence of WAR in buffer is much lower than that in the protein environment as shown in Figure 8. The intensity increase upon binding with HSA can be correlated to the decrease in nonradiative loss of fluorescence due to the caging effect of the protein pocket on the WAR molecule. We can conclude from the above results that HQ probes bind in the same pocket as WAR. If both HQ and WAR exist in the same pocket, there must be some interaction between them if they are close to each other. To clarify this point, we measured the fluorescence spectrum of the binary mixture HSA:7HQ and compared it with that of the ternary mixture WAR:HSA:7HQ. We chose 7HQ because of its fluorescence peak at ca. 500 nm which is due to the excited zwitterionic (Z) species. This peak is distinguished from the WAR fluorescence as shown in Figure 8. It is clear that the intensity of this peak is reduced in the presence of WAR. We have shown recently that fluorescence from the Z tautomer is enhanced in aqueous environments which points to the presence of water inside subdomain IIA.[19] The reduction in its intensity is then a consequence of the presence of WAR in close proximity to 7HQ in which the WAR molecule may replace some of the water molecules that are in contact with the polar sites of 7HQ. We should not rule out the possibility of energy transfer from WAR to 7HQ since the fluorescence peak of WAR at ca. 380 nm overlaps with the absorption peak of the Z tautomer of 7HQ (Figure 7 in ref 19). However, the extinction coefficient of 7HQ at 380 is very small, and our results here indicate that the contribution from energy transfer is negligible. This may be due to the larger effect of 7HQ being less solvated in the presence of WAR and the poor FRET mechanism between WAR and 7HQ.

DISCUSSION

The results presented above provide a picture of HQ binding to HSA. Data from fluorescence spectroscopy, ligand docking, or MD simulations alone leave several points unclear about the details of ligand binding. The combination of all three methods offers a much clearer picture.

Ligand Binding Strength. Regarding the binding strength of different HQ ligands, the experimental values in the low micromolar region are in surprisingly good agreement with the estimated $\Delta G^0_{\mathrm{Bind}}$ of ca. −5.4 kcal/mol from Autodock calculations. The results are effectively within ca. 1 kcal/mol of each other (using the relation $\Delta G^0 = -RT\ \ln(K)$), easily within the margin of error of either approach. Interestingly, the computationally much more expensive MM-PBSA method does not produce binding energies in better, or even equally good, agreement with experiment but also suggests that all three ligands have comparable binding strength. All three methods support the conclusion that the different HQ ligands are moderately strong binders to HSA. None of the four suggested binding pockets were found to produce significantly higher or lower binding free energies for any ligand. These findings are in good agreement with the general ability of HSA to bind a variety of ligands, but without the extremely high affinities typical for, e.g., drug target inhibitor complexes.

Binding Site Flexibility. Simulations both with and without ligands support the picture of HSA as a stable but very flexible protein. The three domains of HSA are capable of substantial relative movement even while their secondary structure remains nearly unchanged. Likewise, binding site amino acid residues in the apoprotein inhabit multiple conformational substates. This does not change upon ligand binding; instead, HQ ligands also exhibit considerable motion within their binding pockets and the ability to move between different binding pockets on the multinanosecond time scale. This points to the dynamical nature of HSA−HQ complexes which is only incompletely described in static X-ray crystal or ligand docking structures but can be understood well from long MD simulations of the system. The picture of a flexible protein with potentially multiple binding sites lined by both hydrophobic and hydrophilic amino acid residues, which can easily adapt their shape to a variety of ligands, again reinforces the nature of HSA as an indiscriminate ligand binder. The lack of a single stable ligand binding pose for HQ ligands indicates that structural flexibility also needs to be taken into account when

dx.doi.org/10.1021/jp311238n | J. Phys. Chem. B 2013, 117, 1062−1074

interpreting their spectroscopic signals. This is apparent in the small decrease of the fluorescence lifetime for Trp214, due to collisional quenching from mobile ligands, while static quenching remains the dominant effect.

Multiple Binding Pockets. Ligand docking results indicate four possible binding pockets over which the suggested binding poses of HQs were distributed. Deciding on which binding pocket is the most likely one for the HQ molecules is difficult from both experiment and theory. From the simulations and docking placements, binding pocket 4 appears to be the least likely since only two binding poses were found there, few direct strong interactions between ligands and pocket 4 were found, and the bound ligands are fairly flexible and solvent exposed. Placements in this pocket are far away from the established ligand binding region in subdomain IIA of HSA, and they may be due to the known effect of ligand docking calculations to produce false positive binding predictions. Still, the potential for protein surface binding of HQ ligands cannot be eliminated based on our data.

A comparison of ligand−Trp214 distances from simulation (Table 5) and fluorescence donor−acceptor distances R_{DA} (Table 6) shows that binding pockets 2 and 3 have distances to Trp in agreement with experiment, if the uncertainty from fluorescence distance measurements is considered. For binding pocket 1, which has the ligand in direct contact to Trp214, one would expect a larger contribution from static quenching and a smaller value for R_{DA}. When comparing pockets 2 and 3, the ligands in the former pocket are always very close to multiple Tyr residues, and for the latter Tyr residues in intermediate distance of ca. 10 Å are found. Only a moderate effect of HQ ligands on Tyr fluorescence is found in experiment, which better agrees to binding in pocket 3. Overall, ligand binding in pocket 3, which is also the preferred binding pocket of the warfarin ligand, is in best agreement to experimental data. We have previously performed a FRET experiment on the HSA−warfarin complex and estimated the Trp214−warfarin distance to be 17 Å as well, which supports this conclusion.[19] The amount of uncertainty in this conclusion should not be understated since both fluorescence and docking and simulation methods are problematic for determining atomic distances, and in addition, ligands can be mobile and moving between different binding positions on the time scale of experiment.

The fact that the experimentally determined number of binding sites m was found to be close to one at first seems at odds with the multiple binding pockets predicted from docking and simulation. However, calculations assume only a single bound ligand, and occupation of one of the binding pockets could well prevent other ligands from binding (negative cooperativity), especially if a mobile ligand is able to transiently occupy multiple binding pockets and thereby block them for additional ligands. In that case, multiple binding pockets would appear as a single binding site on the macroscopic time scale of experiment.

Ligand−Water Interactions. Both solvent distribution functions from experiment (see Figure 6) and the stability of HQ zwitterion tautomers are indicative of the partially solvated nature of the complex binding site. For all four predicted binding pockets, polar amino acid residues lining the binding pocket and the formation of stable hydrogen bonds to solvent in nearly all of the predicted binding poses support this picture. Unlike cases of nonpolar ligands binding hydrophobic binding pockets deep inside a receptor, in HSA ligand binding water clearly plays a role in molecular recognition. This role may be a consequence of the tendency of water molecules inside the protein sites to be ordered with less flexibility compared to bulk water.[20] If this effect goes beyond packing effects and binding site polarity and involves structurally important water molecules, bridging interactions between HQ ligands and protein side chains remain an open question that we plan to address in future studies.

CONCLUSION

In this work we show that several isomeric HQ ligands bind to HSA with moderate binding strength and serve as useful molecular probes to study the nature of HSA binding sites. Ligand docking and molecular dynamics simulations show several different binding pockets on HSA and confirm the very flexible nature of both the HSA apoprotein and HSA−HQ complexes. No unambiguous determination of the actual binding site is possible, but combining molecular modeling and fluorescence spectroscopy data, it appears likely that HQ ligands bind in a binding mode similar to warfarin and interact with the sole Trp residue in HSA as well as several Tyr residues. The likely binding sites contain both hydrophilic and hydrophobic residues and are well solvated even when occupied by a ligand. Our results reaffirm the nature of HSA as a versatile and indiscriminate receptor, capable of binding a variety of ligands by adapting its binding pockets. Computational models are well suited for the task of understanding ligand binding, even in large, dynamic systems, and the often only qualitative nature of their results can be usefully complemented with experimental data.

ASSOCIATED CONTENT

Supporting Information

Additional details about how fluorescence lifetimes and binding constants were obtained, as well as experimental data plots. This information is available free of charge via the Internet at http://pubs.acs.org

AUTHOR INFORMATION

Corresponding Author

*Tel.: (+968) 2414-1468. Fax: (+968) 2414-1469. E-mail: abouzied@squ.edu.om (O.K.A-Z.). E-mail: thomas.steinbrecher@kit.edu (T.B.S.).

Notes

The authors declare no competing financial interest.

ACKNOWLEDGMENTS

The authors would like to thank the Amber community for helpful discussions of MD simulation analysis. T.S. is indebted to the Baden-Württemberg Stiftung for the financial support of this research project by the *Eliteprogramme for Postdocs*. O.K.A-Z. and N.A-L. would like to thank Sultan Qaboos University for financial support (Grant No. IG/SCI/CHEM/12/01).

REFERENCES

(1) Copeland, R. A. *Enzymes: A Practical Introduction to Structure, Mechanism, and Data Analysis*, 2nd ed.; Wiley: New York, 2000.
(2) Berde, C. B.; Hudson, B. S.; Simon, R. D.; Sklar, L. A. *J. Biol. Chem.* **1979**, *254*, 391−400.
(3) Curry, S. *Drug Metab. Pharmacokinet.* **2009**, *4*, 342−357.
(4) He, X. M.; Carter, D. C. *Nature* **1992**, *358*, 209−215.
(5) Carter, D. C.; Ho, J. X. *Adv. Protein Chem.* **1994**, *45*, 153−203.

(6) Petitpas, I.; Bhattacharya, A. A.; Twine, S.; East, M.; Curry, S. *J. Biol. Chem.* **2001**, *276*, 22804−22809.
(7) Sudlow, G.; Birkett, D. J.; Wade, D. N. *Mol. Pharmacol.* **1976**, *12*, 1052−1061.
(8) Colmenarejo, G. *Med. Res. Rev.* **2003**, *3*, 275−301.
(9) Ghuman, J.; Zunszain, P. A.; Petitpas, I.; Bhattacharya, A. A.; Otagiri, M.; Curry, S. *J. Mol. Biol.* **2005**, *353*, 38−52.
(10) Kragh-Hansen, U. *Pharm. Rev.* **1981**, *33*, 17−53.
(11) Peters, T. *Adv. Protein Chem.* **1985**, *37*, 61−245.
(12) Jusko, W. J.; Gretch, M. *Drug Metab. Rev.* **1976**, *5*, 43−140.
(13) Kratz, F. *J. Controlled Release* **2008**, *132*, 171−183.
(14) Kragh-Hansen, U.; Chuang, V. T. G.; Otagiri, M. *Biol. Pharm. Bull.* **2002**, *6*, 695−704.
(15) Sułkowska, A.; Maciazek-Jurczyk, M.; Bojko, B.; Rownicka, J.; Zubik-Skupien, I.; Temba, E.; Pentak, D.; Sulkowski, W. W. *J. Mol. Struct.* **2008**, *881*, 97−106.
(16) Bojko, B.; Sułkowska, A.; Maciazek-Jurczyk, M.; Rownicka, J.; Sulkowski, W. W. *J. Mol. Struct.* **2009**, 332−337.
(17) Shaikh, S. M. T.; Seetharamappa, J.; Kandagal, P. B.; Ashoka, S. J. *J. Mol. Struct.* **2006**, *786*, 46−52.
(18) Al-Lawatia, N.; Steinbrecher, T.; Abou-Zied, O. K. *Proc. SPIE* **2012**, *7576*, D1−D11.
(19) Abou-Zied, O. K.; Al-Lawatia, N. *ChemPhysChem* **2011**, *12*, 270−274.
(20) Qiu, W.; Zhang, L.; Okobiah, O.; Yang, Y.; Wang, L.; Zhong, D.; Zewail, A. H. *J. Phys. Chem. B* **2006**, *110*, 10540−10549.
(21) Kratochwil, N. A.; Huber, W.; Muller, F.; Kansy, M.; Gerber, P. R. *Biochem. Pharmacol.* **2002**, *9*, 1355−1374.
(22) Votano, J. R.; Parham, M.; Hall, L. M.; Hall, L. H.; Kier, L. B.; Oloff, S.; Tropsha, A. *J. Med. Chem.* **2006**, *24*, 7169−7181.
(23) Estrada, E.; Uriarte, E.; Molina, E.; Simon-Manso, Y.; Milne, G. W. A. *J. Chem. Inf. Model.* **2006**, *6*, 2709−2724.
(24) Zsila, F.; Bikadi, Z.; Malik, D.; Hari, P.; Pechan, I.; Berces, A.; Hazai, E. *Bioinformatics* **2011**, *13*, 1806−1813.
(25) Wang, G.; Wang, D.; Li, X.; Lu, Y. *Colloids Surf. B* **2011**, *1*, 272−279.
(26) Wang, C.; Li, Y. *J. Agric. Food Chem.* **2011**, *15*, 8507−8512.
(27) Wang, Q.; Zhang, Y.; Sun, H.; Chen, H.; Chen, X. *J. Lumin.* **2011**, *2*, 206−211.
(28) Tousi, S. H.; Saberi, M. R.; Chamani, J. *Rom. J. Biochem.* **2011**, *2*, 135−175.
(29) Wang, X.; Xie, X.; Ren, C.; Yang, Y.; Xu, X.; Chen, X. *Food Chem.* **2011**, *2*, 705−710.
(30) Daneshgar, P.; Moosavi-Movahedi, A. A.; Norouzi, P.; Ganjali, M. R.; Madadkar-Sobhani, A.; Saboury, A. A. *Int. J. Biol. Macromol.* **2009**, *2*, 129−134.
(31) Yang, Q.; Zhou, X.; Chen, X. *J. Lumin.* **2011**, *4*, 581−586.
(32) Kaliszan, R.; Noctor, T.; Wainer, I. W. *Chromatographia* **1992**, *33*, 546−550.
(33) Colmenarejo, G.; Alvarez-Pedraglio, A.; Lavandera, J. L. *J. Med. Chem.* **2001**, *44*, 4370−4378.
(34) Hall, L. M.; Hall, L. H.; Kier, L. B. *J. Chem. Inf. Comp.* **2003**, *43*, 2120−2128.
(35) Li, J.; Zhu, X.; Yang, C.; Shi, R. *J. Mol. Model.* **2010**, *4*, 789−798.
(36) Paris, G.; Kraszewski, S.; Ramseyer, C.; Enescu, M. *Biopolymers* **2012**, *97*, 889−898.
(37) Jana, S.; Dalapati, S.; Ghosh, S.; Guchhait, N. *Biopolymers* **2012**, *97*, 766−777.
(38) Deeb, O.; Rosales-Hernandez, M. C.; Gomez-Castro, C.; Garduno-Juarez, R.; Correa-Basurto, J. *Biopolymers* **2010**, *93*, 161−170.
(39) Liu, H.; Bao, W.; Ding, H.; Jang, J.; Zou, G. *J. Phys. Chem. B* **2010**, *114*, 12938−12947.
(40) Fujiwara, S.; Amisaki, T. *Chem. Pharm. Bull.* **2011**, *7*, 860−867.
(41) Morris, G. M.; Goodsell, D. S.; Halliday, R. S.; Huey, R.; Hart, W. E.; Belew, R. K.; Olson, A. J. *J. Comput. Chem.* **1998**, *19*, 1639−1662.
(42) Salomon-Ferrer, R.; Case, D. A.; Walker, R. C. *Wiley Interdiscip. Rev.: Comput. Mol. Sci.* **2012**, DOI: 10.1002/wcms.1121.
(43) Case, D. A. et al. *AMBER11*; University of California: San Francisco, 2010.
(44) Perez, A.; Marchan, I.; Svozil, D.; Sponer, J.; Cheatham, T.; Laughton, C.; Orozco, M. *Biophys. J.* **2007**, *92*, 3817−3829.
(45) Banáš, P.; Hollas, D.; Zgarbová, M.; Jurecka, P.; Orozco, M.; Cheatham, T., III; Šponer, J.; Otyepka, M. *J. Chem. Theory. Comput.* **2010**, *6*, 3836−3849.
(46) Zgarbova, M.; Otyepka, M.; Sponer, J.; Mladek, A.; Banas, P.; Cheatham, T.; Jurecka, P. *J. Chem. Theory Comput.* **2011**, *7*, 2886−2902.
(47) Joung, S.; Cheatham, T., III *J. Phys. Chem. B* **2008**, *112*, 9020−9041.
(48) Joung, I.; Cheatham, T., III *J. Phys. Chem. B* **2009**, *113*, 13279−13290.
(49) Hornak, V.; Abel, R.; Okur, A.; Strockbine, B.; Roitberg, A.; Simmerling, C. *Proteins* **2006**, *65*, 712−725.
(50) Horn, H.; Swope, W.; Pitera, J.; Madura, J.; Dick, T.; Hura, G.; Head-Gordon, T. *J. Chem. Phys.* **2004**, *120*, 9665−9678.
(51) Horn, H.; Swope, W.; Pitera, J. *J. Chem. Phys.* **2005**, *123*, 194504.
(52) Wang, J.; Wolf, R.; Caldwell, J.; Kollamn, P.; Case, D. *J. Comput. Chem.* **2004**, *25*, 1157−1174.
(53) Bayly, C.; Cieplak, P.; Cornell, W.; Kollman, P. *J. Phys. Chem.* **1993**, *97*, 10269.
(54) Ryckaert, J.-P.; Ciccotti, G.; Berendsen, H. *J. Comput. Phys.* **1977**, *23*, 327−341.
(55) Miyamoto, S.; Kollman, P. *J. Comput. Chem.* **1992**, *13*, 952−962.
(56) Darden, T.; York, D.; Pedersen, L. *J. Chem. Phys.* **1993**, *98*, 10089−10092.
(57) Essmann, U.; Perera, L.; Berkowitz, M.; Darden, T.; Lee, H.; Pedersen, L. *J. Chem. Phys.* **1995**, *103*, 8577−8593.
(58) Crowley, M.; Darden, T.; Cheatham, T., III; Deerfield, D., II *J. Supercomput.* **1997**, *11*, 255−278.
(59) Salomon-Ferrer, R.; Goetz, A. W.; D., P.; LeGrand, S.; Walker, R. C. *J. Chem. Theory Comput.* **2012**, in preparation.
(60) LeGrand, S.; Goetz, A. W.; Walker, R. C. *Comput. Phys. Commun.* **2012**, in press.
(61) Humphrey, W.; Dalke, A.; Schulten, K. *J. Mol. Graph. Model.* **1996**, *14*, 33−38.
(62) Frishman, D.; Argos, P. *Protein: Struct. Funct. Genet.* **1995**, *23*, 566−579.
(63) *Persistence of Vision Raytracer*. Persistence of Vision Pty. Ltd.: Williamstown, Victoria, Australia, 2004.
(64) Putnam, F. W., Ed. *The Plasma Proteins*, 2nd ed.; Academic Press, New York, 1975; pp 133−181.
(65) James, D. R.; Siemiarczuk, A.; Ware, W. R. *Rev. Sci. Instrum.* **1992**, *63*, 1710−1716.
(66) Lakowicz, J. R. *Principles of Fluorescence Spectroscopy*, 3rd ed.; Springer: New York, 2006.
(67) Abou-Zied, O. K.; Al-Shihi, O. I. K. *J. Am. Chem. Soc.* **2008**, *130*, 10793−10801.
(68) Royer, C. A. *Chem. Rev.* **2006**, *106*, 1769.
(69) Petitpas, I.; Grune, T.; Bhattacharya, A. A.; Curry, S. *J. Mol. Biol.* **2001**, *314*, 955−960.
(70) Hein, K. L.; Kragh-Hansen, U.; Morth, J. P.; Jeppesen, M. D.; Otzen, D.; Moller, J. V.; Nissen, P. *J. Struct. Biol.* **2010**, *171*, 353−360.
(71) Kollman, P. *Chem. Rev.* **1993**, *93*, 2395−2417.
(72) Reddy, M. R.; Erion, M. D.; Agarwal, A. *Rev. Comp. Chem.* **2000**, *16*, 217−304.
(73) Wang, W.; Donini, O.; Reyes, C. M.; Kollman, P. A. *Annu. Rev. Biophys. Biomol. Struct.* **2001**, *30*, 211−243.
(74) Lazaridis, T. *Curr. Org. Chem* **2002**, *6*, 1319−1332.
(75) Simonson, T.; Archontis, G.; Karplus, M. *Acc. Chem. Res.* **2002**, *35*, 430−437.
(76) Brandsdal, B. O.; Osterberg, F.; Almlof, M.; Feierberg, I.; Luzhkov, V. B.; Åqvist, J. *Free energy calculations and ligand binding*; Academic Press Inc.: San Diego, 2003; Vol. *66*.
(77) Foloppe, N.; Hubbard, R. *Curr. Med. Chem.* **2006**, *13*, 3583−3608.

(78) Jorgensen, W. L. *Science* **2004**, *303*, 1813−1818.
(79) Shirts, M. R.; Mobley, D. L.; Brown, S. P. Free energy calculations in structure-based drug design. *Structure Based Drug Design*; Cambridge University Press: New York, 2010.
(80) Li, D.; Brüschweiler, R. *Angew. Chem., Int. Ed.* **2010**, *49*, 6778−6780.
(81) Sułkowska, A. *J. Mol. Struct.* **2002**, *614*, 227−232.
(82) Förster, T. *Discuss. Faraday Soc.* **1959**, *27*, 7−17.
(83) Berezin, M. Y.; Achilefu, S. *Chem. Rev.* **2010**, *110*, 2641−2684.
(84) Ware, W. R. *J. Phys. Chem.* **1962**, *66*, 455−458.
(85) Connors, K. A. *Binding Constants. The Measurements of Molecular Complex Stability*; Wiley: New York, 1987.
(86) Il'ichev, Y. V.; Perry, J. L.; Simon, J. D. *J. Phys. Chem. B* **2002**, *106*, 460−465.